

# Single wall carbon nanotubes as coherent plasmon generators

I. V. Bondarev

*Department of Physics, North Carolina Central University, Durham, NC 27707, USA*

The possibility of low-energy surface plasmon amplification by optically excited excitons in small-diameter single wall carbon nanotubes is theoretically demonstrated. The nonradiative exciton-plasmon energy transfer causes the buildup of the macroscopic population numbers of coherent localized surface plasmons associated with high-intensity coherent local fields formed at nanoscale throughout the nanotube surface. These strong local fields can be used in a variety of new optoelectronic applications of carbon nanotubes, including near-field nonlinear-optical probing and sensing, optical switching, enhanced electromagnetic absorption, and materials nanoscale modification.

Single wall carbon nanotubes (CNs) — graphene sheets rolled-up into cylinders of  $\sim 1-10$  nm in diameter and  $\sim 1 \mu\text{m}$  up to  $\sim 1$  cm in length [1–3] — are shown to be very useful as miniaturized electromechanical and chemical devices [4], scanning probe devices [5, 6], and nanomaterials for macroscopic composites [7–9]. The area of their potential applications was recently expanded to nanophotonics [10–15] after the demonstration of controllable single-atom incapsulation into single-walled CNs [16], and even to quantum cryptography since the experimental evidence was reported for quantum correlations in the photoluminescence spectra of individual nanotubes [17].

The true potential of CN-based optoelectronic device applications lies in the ability to tune their properties in a precisely controllable way. In particular, optical properties of semiconducting CNs originate from excitons, and may be tuned by either electrostatic doping [15, 18, 19], or via the quantum confined Stark effect (QCSE) by means of an electrostatic field applied perpendicular to the nanotube axis [20, 21]. In both cases the exciton properties are mediated by collective plasmon excitations in CNs [22, 23]. In the case of the perpendicularly applied electrostatic field (Fig. 1), we have shown recently that the QCSE allows one to control the exciton-interband-plasmon coupling in individual undoped CNs and their optical absorption properties, both linear [20] and nonlinear [21], accordingly.

The formation of coupled exciton-plasmon excitations can be viewed as an additional non-radiative channel (in addition to phonons [24] and defects [25]) for the exciton relaxation in CNs, whereby the optically excited exciton decays into low-energy (inter-band) plasmons. In so doing, the exciton generates the quanta of plasma oscillations on the CN surface, on the one hand, and this shortens its lifetime, on the other. Thus, by varying the exciton-plasmon coupling strength using the QCSE one controls both the radiative emission from an individual CN and surface electric field fluctuations due to the exciton decay into plasmons on the CN surface. This latter phenomenon is pretty much similar to the SPASER effect (Surface Plasmon Amplification by Stimulated Emission of Radiation) reported earlier for hybrid metal-semiconductor-dielectric nanosystems [26], and is the focus of the studies here for individual small-diameter ( $\sim 1$  nm) CNs. The non-radiative exciton-to-

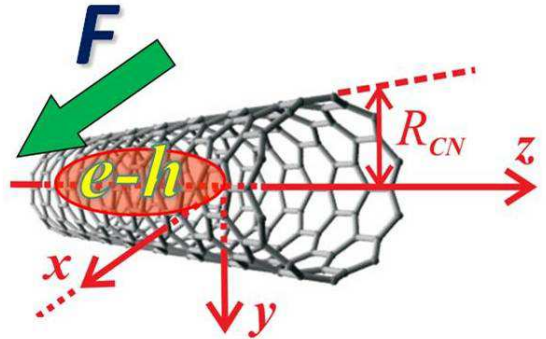


FIG. 1: (Color online) The geometry of the problem.

plasmon energy transfer is shown to result in the large population numbers of coherent surface plasmons associated with high-intensity coherent oscillating fields concentrated at nanoscale across the CN diameter along the CN length. These strong local fields can be used in a variety of new CN based optoelectronic applications, including near-field nonlinear-optical probing and sensing, optical switching, enhanced electromagnetic absorption, and materials nanoscale modification.

Longitudinal excitons, for which both the transition dipole moment and the momentum vector are directed along the nanotube axis ( $z$  axis of the problem; cylindrical coordinates are used — see Fig. 1), are excited by the external electromagnetic (EM) radiation polarized along the CN axis [27]. These are shown to be able to couple to neighboring low-energy interband surface plasmon modes [11, 20], such as the exciton  $E_{11}$  and the plasmon  $P_{11}$  in Fig. 2 (a) for the (11,0) CN (taken as an example). Figure 2 (b) shows the corresponding exciton-plasmon dispersion relation (derived in Ref. [20]) as a function of the perpendicular electrostatic field applied and longitudinal momentum. We see the anti-crossing  $\sim 0.1$  eV, both in the energy-momentum plane and in the energy-field plane, revealing the QCSE as an efficient tool to control the exciton-plasmon coupling strength in individual CNs.

When the exciton is excited and the CN surface EM field subsystem is in the vacuum state, the time-dependent wave function of the whole system "exciton +

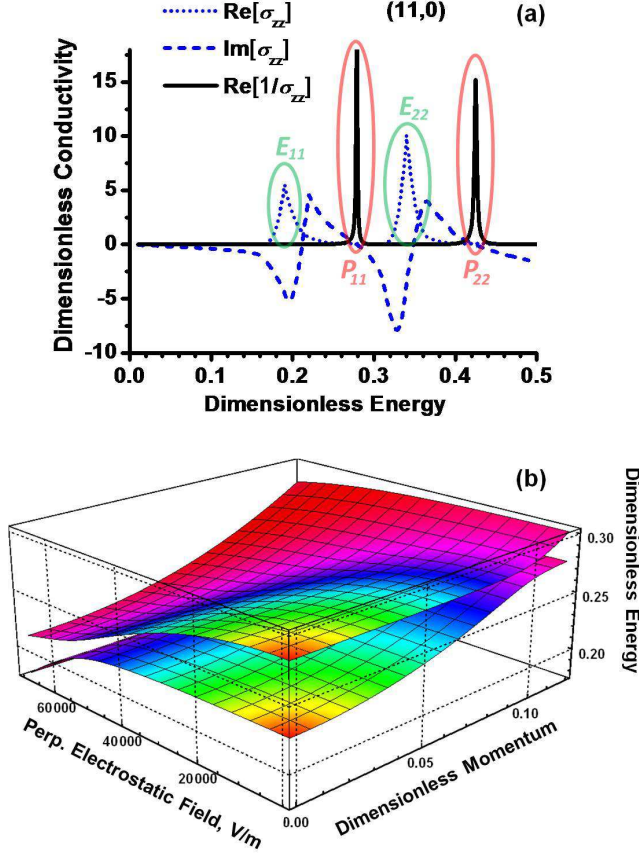


FIG. 2: (Color online) Calculations for the (11,0) CN. (a) Fragment of the energy dependence of the dimensionless (normalized by  $e^2/2\pi\hbar$ ) axial surface conductivity  $\sigma_{zz}$  along the CN axis [20]. Ovals mark exciton ( $E_{11}$ ,  $E_{22}$ ) and interband plasmon ( $P_{11}$ ,  $P_{22}$ ) excitations [peaks of  $\text{Re}\sigma_{zz}$  and  $\text{Re}(1/\sigma_{zz})$ , respectively]. (b) Exciton-plasmon dispersion relation as a function of the perpendicular electrostatic field applied (see Fig. 1) and longitudinal momentum for the lowest bright exciton [ $E_{11}$  in (a)] when coupled to the nearest interband plasmon [ $P_{11}$  in (a)]. Dimensionless momentum and dimensionless energy are defined as  $3b[\text{Momentum}]/(2\pi\hbar)$  and  $[\text{Energy}]/2\gamma_0$ , respectively, where  $b = 1.42 \text{ \AA}$  is the C-C interatomic distance and  $\gamma_0 = 2.7 \text{ eV}$  is the C-C overlap integral.

surface EM field” is of the form

$$|\psi(t)\rangle = \sum_{\mathbf{k}, f} C_f(\mathbf{k}, t) e^{-i\tilde{E}_f(\mathbf{k})t/\hbar} |\{1_f(\mathbf{k})\}\rangle_{ex} |\{0\}\rangle \quad (1)$$

$$+ \sum_{\mathbf{k}} \int_0^\infty d\omega C(\mathbf{k}, \omega, t) e^{-i\omega t} |\{0\}\rangle_{ex} |\{1(\mathbf{k}, \omega)\}\rangle.$$

Here,  $|\{1_f(\mathbf{k})\}\rangle_{ex}$  is the single-quantum Fock state with one  $f$ -internal-state exciton excited of quasi-momentum  $\mathbf{k} = \{k_\varphi, k_z\}$  with quantized  $k_\varphi$  component (transverse quantization that results in electron-hole subbands) and continuous  $k_z$  component representing the longitudinal motion of the exciton. The excited single-quantum state  $|\{1(\mathbf{k}, \omega)\}\rangle$  represents longitudinally polarized surface EM mode of frequency  $\omega$  (the plasmon). The re-

spective vacuum states are  $|\{0\}\rangle_{ex}$  for the exciton subsystem and  $|\{0\}\rangle$  for the surface EM field subsystem. The coefficients  $C_f(\mathbf{k}, t)$  and  $C(\mathbf{k}, \omega, t)$  stand for the population probability amplitudes of the exciton subsystem and field subsystem, respectively. The exciton energy is of the form  $\tilde{E}_f(\mathbf{k}) = E_f(\mathbf{k}) - i\hbar/\tau$ , where  $E_f(\mathbf{k}) = E_{exc}^{(f)}(k_\varphi) + \hbar^2 k_z^2 / 2M_{ex}(k_\varphi)$  stands for the total energy of the  $f$ -internal-state exciton and  $\tau$  represents the phenomenological relaxation time to account for all possible (but into plasmons) slow exciton relaxation processes (normally attributed to the exciton-phonon scattering [20, 24]). The energy  $E_f(\mathbf{k})$  consists of the exciton excitation energy  $E_{exc}^{(f)}(k_\varphi) = E_g(k_\varphi) + E_b^{(f)}(k_\varphi)$ , where  $E_g(k_\varphi) = \varepsilon_e(k_\varphi) + \varepsilon_h(k_\varphi)$  is the band gap with  $\varepsilon_{e,h}$  being the transversely quantized azimuthal electron-hole subbands,  $E_b^{(f)}$  is the (negative) binding energy of the exciton, and the kinetic energy of the translational longitudinal motion of the exciton with the effective mass  $M_{ex} = m_e + m_h$ , where  $m_e$  and  $m_h$  are the (subband-dependent) electron and hole effective masses.

The time dependent Schrödinger equation with the Hamiltonian of the whole system ”exciton + surface EM field” applied on the wave function (1) results in the set of the coupled differential equations for  $C_f(\mathbf{k}, t)$  and  $C(\mathbf{k}, \omega, t)$  as follows [20]

$$i\hbar \dot{C}_f(\mathbf{k}, t) e^{-i\tilde{E}_f(\mathbf{k})t/\hbar} = \int_0^\infty d\omega g_f^{(+)}(\mathbf{k}, \mathbf{k}, \omega) C(\mathbf{k}, \omega, t) e^{-i\omega t},$$

$$i\hbar \dot{C}(\mathbf{k}, \omega, t) e^{-i\omega t} = \sum_f [g_f^{(+)}(\mathbf{k}, \mathbf{k}, \omega)]^* C_f(\mathbf{k}, t) e^{-i\tilde{E}_f(\mathbf{k})t/\hbar}.$$

Here, the interaction matrix element squared is given by

$$|g_f^{(+)}(\mathbf{k}, \mathbf{k}, \omega)|^2 = \frac{\hbar S_0 |d_z^f|^2 \omega^3}{16\pi^3 e^2 R_{CN}^2} \text{Re} \frac{1}{\sigma_{zz}(\mathbf{k}, \omega)}, \quad (2)$$

where  $d_z^f = \sum_{\mathbf{n}} \langle 0 | (\hat{\mathbf{d}}_{\mathbf{n}})_z | f \rangle$  with  $\langle 0 | (\hat{\mathbf{d}}_{\mathbf{n}})_z | f \rangle$  being the electric dipole transition matrix element where the  $f$ -internal-state exciton is excited in the lattice site  $\mathbf{n}$  of the CN surface,  $\sigma_{zz}$  stands for the CN surface axial conductivity with  $\text{Re}(1/\sigma_{zz})$  representing the plasmon density of states [DOS, see Fig. 2 (a)],  $R_{CN}$  is the CN radius, and  $S_0 = (3\sqrt{3}/4)b^2$  is the area of an elementary equilateral triangle selected around each carbon atom in a way to cover the entire CN surface,  $b = 1.42 \text{ \AA}$  is the C-C interatomic distance.

In terms of the probability amplitudes  $C_f(\mathbf{k}, t)$  and  $C(\mathbf{k}, \omega, t)$ , the exciton emission intensity distribution to generate plasmons is given by the final state probability at long times corresponding to the decay of all initially excited excitons, i.e.,  $I(\mathbf{k}, \omega) = |C(\mathbf{k}, \omega, t \rightarrow \infty)|^2$ . This is related to the exciton probability amplitude  $C_f(\mathbf{k}, t)$  according to the equations above, and thereby is also associated with the exciton absorption [20]. The peak intensity represents the long-time plasmon population generated by excitons with the momentum  $\mathbf{k}$ .

Plasma oscillations generated by the non-radiative exciton decay into the nearest inter-band plasmon mode

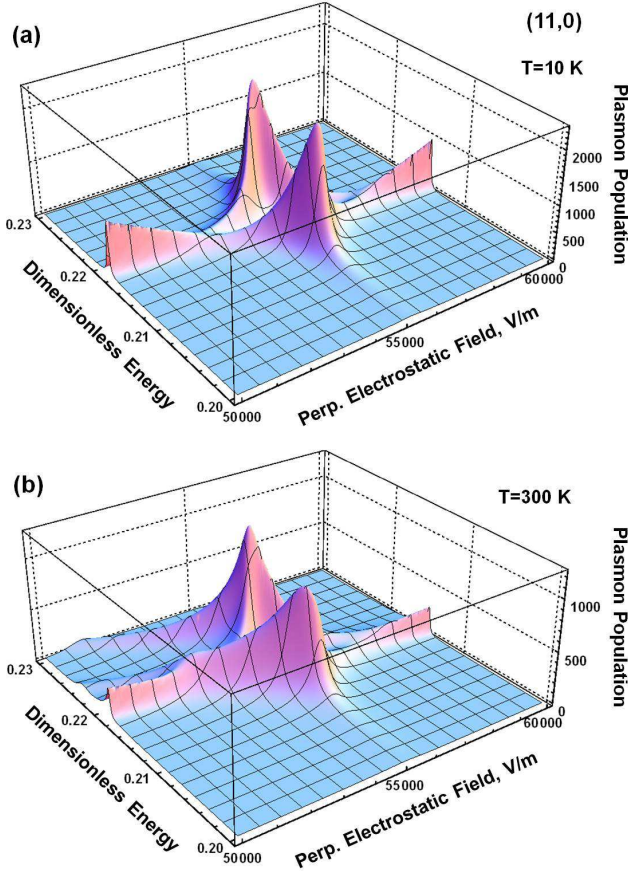


FIG. 3: (Color online) Low (a) and high (b) longitudinal-momentum-averaged plasmon population (arb. units) for the non-radiative decay of the 1st bright exciton in the (11,0) CN. See Fig. 2 caption for the dimensionless energy.

[Fig. 2 (a)] can be viewed as *standing* charge density waves due to the periodic opposite-phase displacements of the electron shells with respect to the ion cores in the neighboring elementary cells on the CN surface. Such periodic displacements induce local coherent oscillating electric fields of zero mean, but non-zero mean-square magnitude, concentrated at nanoscale across the CN diameter throughout the CN length. The mean-square field magnitude can be calculated as the observable of the quantum electrodynamical longitudinal-electric-field operator (see Ref. [20]),  $E_z^2(\mathbf{n}) = \langle [-\nabla_{\mathbf{n}} \hat{\phi}(\mathbf{n})]_z^2 \rangle$ , at the lattice site  $\mathbf{n} = \{R_{CN}, \varphi_n, z_n\}$  of the CN surface in the state with the wave function (1). This results in

$$E_z^2(\mathbf{n}) = \frac{\hbar L}{(2\pi c)^2 R_{CN}} \sum_{\mathbf{k}=k_\varphi, k_z} f_{ex}(\mathbf{k}, T) \quad (3)$$

$$\times \int_0^\infty d\omega \omega^3 \text{Re} \frac{1}{\sigma_{zz}(\mathbf{k}, \omega)} \left[ N(\mathbf{k}, \omega) + \frac{1}{2} \right],$$

where  $N(\mathbf{k}, \omega) = (8\pi c/L)I(\mathbf{k}, \omega)$  is the number of plasmons generated by excitons with the momentum  $\mathbf{k}$  of the 1st Brillouin zone on the surface of the tubule of length  $L$ ,

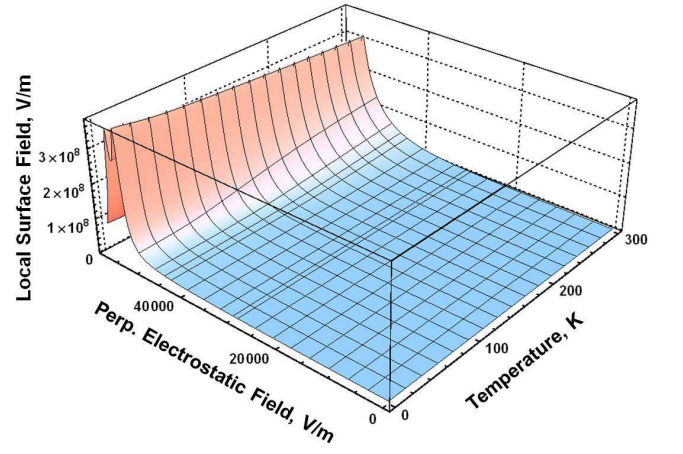


FIG. 4: (Color online) Local surface field amplitude,  $E_z$ , as a function of temperature and perpendicular electrostatic field applied, given by Eq. (3) for plasmons generated by the non-radiative decay of the 1st bright exciton in the (11,0) CN.

and  $f_{ex}(\mathbf{k}, T) = \exp[-\hbar^2 k_z^2 / 2M_{ex}(k_\varphi)k_B T] / Q_{ex}$  is the exciton momentum distribution function with the partition function  $Q_{ex}(T) = \sum_{\mathbf{k}} \exp[-\hbar^2 k_z^2 / 2M_{ex}(k_\varphi)k_B T]$ .

Equation (3) tells that in order to produce strong local mean-square fields, the exciton non-radiative emission resonance [given by  $I(\mathbf{k}, \omega \sim E_{exc})$ ] must overlap with the energy  $E_p$  of the neighboring plasmon DOS resonance {the peak of  $\text{Re}[1/\sigma_{zz}(\omega \sim E_p)]$ }. By way of example of the (11,0) CN in Fig. 2, we see that this can be achieved by carefully tuning the exciton excitation energy  $E_{exc}$  and the nearest inter-band plasmon energy  $E_p$  by means of the QCSE. As this takes place, both  $E_{exc}$  and  $E_p$  experience red shift with increasing perpendicular electrostatic field. However, the red shift of  $E_{exc}$  is very small [barely seen in the constant momenta energy-field planes in Fig. 2 (b)] due to the negative field-dependent contribution of the exciton binding energy  $E_b$  [20]. As a consequence,  $E_{exc}$  and  $E_p$  [ $E_{11}$  and  $P_{11}$  in Fig. 2 (a)] approach as the field increases, pushing the coupled exciton-plasmon system into the strong coupling regime where all of the optically excited excitons decay non-radiatively to generate inter-band (same band) plasmons, yielding the peak optical absorption at the same time. As the temperature grows up, higher momenta excitons start contributing to the process, lowering the field necessary to achieve the strong coupling regime [blue contrast in Fig. 2 (b)].

Figure 3 shows plasmon population numbers averaged over the longitudinal momentum distribution [28],  $\sum_{k_z} f_{ex}(\mathbf{k}, T)N(\mathbf{k}, \omega)$ , also representing optical absorption by excitons, calculated at low and high temperatures for the first bright exciton in the (11,0) CN with  $E_{exc}$  and  $E_p$  being tuned using the QCSE. The same exciton-plasmon parameters and their perpendicular-electrostatic-field dependences are used as those in Ref. [20] ( $E_{exc} = 1.21$  eV,  $E_b = -0.76$  eV,  $E_p = 1.51$  eV in the zero field, and  $\tau = \tau_{ph} = 30$  fs to account for the

exciton-phonon relaxation [24]). We see the dramatic increase in the peak intensities, both at low and at high temperatures, accompanied by Rabi splitting as the field drives the exciton-plasmon system into the strong coupling regime, whereby the effective plasmon generation starts. Temperature generally smoothens the effect due to higher momenta excitons contributing to the process.

Large plasmon population numbers are, according to Eq. (3), associated with coherent oscillating fields concentrated locally throughout the CN surface. Figure 4 shows the calculations for the (11,0) nanotube. Huge local surface fields  $\sim 10^8$  V/m, just a few orders of magnitude less than intra-atomic fields, are created under the resonance conditions. The effect slightly decreases with temperature, but it starts at lower electrostatic fields due to the higher momenta excitons contribution to the plasmon generation. Strong local surface fields created are the result of the efficient energy conversion mechanism, whereby the external radiation energy absorbed to excite excitons transfers into the energy of localized high-intensity coherent optical-frequency fields of charge plasma oscillations. The process can be controlled

by fine-tuning the exciton-plasmon coupling strength by means of the QCSE and by varying the temperature.

The effect presented here for *individual* single wall CNs is analogous to the SPASER effect reported earlier for hybrid metal-semiconductor-dielectric nanostructures [26]. The effect is universal as it originates from the transverse quantization of electronic degrees of freedom in quasi-1D systems. It can manifest itself in densely packed aligned nanotube films as well, both through plasmon enhanced inter-tube Casimir interactions [ $N = 0$ -term in Eq. (3)], as it is recently demonstrated for double wall CN systems [29], and through the exciton-to-plasmon energy transfer tuned by means of the QCSE. In the latter case, plasmon-induced coherent local surface fields can be used in a variety of new tunable optoelectronic applications with both individual nanotubes and nanotube composites, such as near-field nonlinear-optical probing and sensing, optical switching, enhanced electromagnetic absorption, and materials nanoscale modification.

Support from NSF (ECCS-1045661 & HRD-0833184), NASA (NNX09AV07A), and ARO (W911NF-11-1-0189) is gratefully acknowledged.

- 
- [1] R.Saito, G.Dresselhaus, and M.S.Dresselhaus, *Science of Fullerenes and Carbon Nanotubes* (Imperial College Press, London, 1998).
- [2] S.M.Huang, B.Maynor, X.Y.Cai, and J.Liu, *Advanced Materials* **15**, 1651 (2003).
- [3] L.X.Zheng, M.J.O'Connell, S.K.Doorn, X.Z.Liao, Y.H.Zhao, E.A.Akhadov, M.A.Hoffbauer, B.J.Roop, Q.X.Jia, R.C.Dye, D.E.Peterson, S.M.Huang, J.Liu and Y.T.Zhu, *Nature Mat.* **3**, 673 (2004).
- [4] R.H.Baughman, A.A.Zakhidov, and W.A. de Heer, *Science* **297**, 787 (2002).
- [5] A.Popescu, L.M.Woods, and I.V.Bondarev, *Nanotechnology* **19**, 435702 (2008).
- [6] A.Popescu and L.M.Woods, *Appl. Phys. Lett.* **95**, 203507 (2009).
- [7] Z.-P.Yang, L.Ci, J.A.Bur, S.-Y.Lin, and P.M.Ajayan, *NanoLett.* **8**, 446 (2008).
- [8] J.E.Trancik, S.C.Barton, and J.Hone, *NanoLett.* **8**, 982 (2008).
- [9] F.J.Garcia-Vidal, J.M.Pitarke, and J.B.Pendry, *Phys. Rev. B* **58**, 6783 (1998).
- [10] I.V.Bondarev, *J. Comp. Theor. Nanosci.* **7**, 1673 (2010).
- [11] I.V.Bondarev, K.Tatur, and L.M.Woods, *Opt. Commun.* **282**, 661 (2009).
- [12] I.V.Bondarev and B.Vlahovic, *Phys. Rev. B* **75**, 033402 (2007); *ibid.* **74**, 073401 (2006).
- [13] F.Xia, M.Steiner, Y.-M.Lin, and Ph.Avouris, *Nature Nanotech.* **6**, 609 (2008).
- [14] J.-H.Han, G.L.C.Paulus, R.Maruyama, D.A.Heller, W.-J.Kim, P.W.Barone, C.Y.Lee, J.H.Choi, M.-H.Ham, C.Song, C.Fantini, and M.S.Strano, *Nature Materials* **9**, 833 (2010).
- [15] T.Hertel, *Nature Photonics* **4**, 77 (2010); T.Mueller, M.Kinoshita, M.Steiner, V.Perebeinos, A.A.Bol, D.B.Farmer, and Ph.Avouris, *Nature Nanotech.* **5**, 27 (2010).
- [16] G.-H.Jeong, A.A.Farajian, R.Hatakeyama, T.Hirata, T.Yaguchi, K.Tohji, H.Mizuseki, and Y.Kawazoe, *Phys. Rev. B* **68**, 075410 (2003); *Thin Solid Films* **435**, 307 (2003).
- [17] A.Högele, Ch.Galland, M.Winger, and A.Imamoğlu, *Phys. Rev. Lett.* **100**, 217401 (2008).
- [18] C.D.Spataru and F.Léonard, *Phys. Rev. Lett.* **104**, 177402 (2010).
- [19] M.Steiner, M.Freitag, V.Perebeinos, A.Naumov, J.P.Small, A.A.Bol, and Ph.Avouris, *NanoLett.* **9**, 3477 (2009).
- [20] I.V.Bondarev, L.M.Woods, and K.Tatur, *Phys. Rev. B* **80**, 085407 (2009).
- [21] I.V.Bondarev, *Phys. Rev. B* **83**, 153409 (2011); *Phys. Stat. Sol. B* **248**, 468 (2011); *Superlattices and Microstructures* **49**, 217 (2011).
- [22] C.Kramberger, R.Hambach, C.Giorgetti, M.H.Rümmeli, M.Knupfer, J.Fink, B.Büchner, L.Reining, E.Einarsson, S.Maruyama, F.Sottile, K.Hannewald, V.Olevano, A.G.Marinopoulos, and T.Pichler, *Phys. Rev. Lett.* **100**, 196803 (2008).
- [23] T.Pichler, M.Knupfer, M.S.Golden, J.Fink, A.Rinzler, and R.E.Smalley, *Phys.Rev. Lett.* **80**, 4729 (1998).
- [24] V.Perebeinos, J.Tersoff, and Ph.Avouris, *Phys. Rev. Lett.* **94**, 027402 (2005).
- [25] A.Hagen, M.Steiner, M.B.Raschke, C.Lienau, T.Hertel, H.Qian, A.J.Meixner, and A.Hartschuh, *Phys. Rev. Lett.* **95**, 197401 (2005).
- [26] D.J.Bergman and M.I.Stockman, *Phys. Rev. Lett.* **90**, 027402 (2003).
- [27] T.Ando, *J. Phys. Soc. Jpn.* **74**, 777 (2005).
- [28]  $\sigma_{zz}(\mathbf{k}, \omega) = \sigma_{zz}(k_{\varphi}, \omega)$  is assumed for the conductivity; weak longitudinal spatial dispersion is neglected [20].
- [29] A.Popescu, L.M.Woods, and I.V.Bondarev, *Phys. Rev. B* **83**, 081406(R) (2011).